Evaluation of Dynamic Mechanical and Thermal Behavior of HDPE Reinforced with MWCNT/h-BNNP: An Attempt to Find Possible Substitute for a Metallic Knee in Transfemoral Prosthesis

Nitesh Dhar Badgayan[1,2] · Santosh Kumar Sahu[3] · Sutanu Samanta[2] ·
P. S. Rama Sreekanth[4]

Abstract

Nanotechnology has extended applications of conventional engineering plastics like high-density polyethylene (HDPE) to different biomedical implants such as articular cartilage and fracture fixation plates. However, applications in a load-bearing element like a prosthetic knee require estimation of static, dynamic mechanical, and variation of mechanical properties with temperature. The current work reports on the application of HDPE-based nanocomposite as a possible substitute for a metallic knee in a prosthetic leg. HDPE was reinforced with multiwalled carbon nanotubes (MWCNTs)-1D and boron nitride nanoplatelets (h-BNNPs)-2D to form different composites and hybrids. The preparation route followed the mechanical mixing tandem by curing in a vacuum oven. Dynamic mechanical thermal analysis (DMTA) results confirmed the best elastic and damping property by 0.1 MWCNT composite. The mechanical properties like hardness, impact toughness, and stiffness of 0.25 MWCNT/0.15 h-BNNP were observed to increase by 172 %, 190 %, and 50 % in comparison with pure HDPE. A similar observation was noted during the evaluation of thermal conductivity, thermal stability, and %crystallinity. A modified Halpin–Tsai and Hamilton–Crosser model was used to predict the stiffness and thermal conductivity of composites. The test results confirmed 0.25 MWCNT/0.15 h-BNNP as a potential possible substitute for a metallic knee in a transfemoral prosthesis.

Keywords Differential scanning calorimetry · h-BNNPS · MWCNTs · Polymer-matrix composites · Storage modulus · Young's modulus

✉ P. S. Rama Sreekanth
  happyshrikanth@gmail.com

Extended author information available on the last page of the article

1 Introduction

The advent of nanotechnology has widened the scope of polymer to the diverse field of application in both engineering and medical. Concerning medical applications of polymers, they have successfully replaced traditional metallic implants in total hip replacement to the growing of a synthetic trachea [1, 2]. The potential of polymers further exalted by reinforcing it with nanofillers and forming polymer hybrid nanocomposites which each one of the individual fillers used as reinforcement exhibits synergistic effects leading to superior performance. High-density polyethylene (HDPE)-based hybrid nanocomposite has found application in biomedical implants and also areas wherein dynamic loading is prevalent [3]. However, it has immanent loopholes like poor damping abilities when subjected to variable loading at a temperature sweep, poor impact strength which restricts its applications in certain areas. A prosthetic leg is one of such case which is subjected to a complex set of dynamic load and impact load and it is also subjected to temperature variation. Currently, there are multifarious variants of prosthetic legs available in the global market beginning from a simple polymer prosthetic leg to a complex microprocessor-controlled prosthetic [4]. In both the cases, the knee joint is a metal which is generally titanium and titanium alloy. The application of metallic material adds on to the weight and makes the prosthetic heavy apart from consideration of machining economics and time to market which increases the final cost at dispense. In this context, the inherently lightweight, corrosion-resistant polymers can suitably replace the metallic knee. However, materials for prosthetic knee must possess properties such as high toughness, lubricity, wear resistance, and damping abilities with temperature variation. But polymers can neither withstand temperature-varied dynamic load nor dissipate the same and it is also apparently weak in absorbing impact loads. In this current work, an attempt is made to reinforce HDPE with suitable nanofillers to augment and exalt the required properties. The properties of specific interests are the damping abilities (dynamic properties) with temperature variation besides others. The techniques like Dynamic Mechanical Thermal Analysis (DMTA) successfully characterize dynamic properties like storage modulus, loss modulus, and Tanδ during a frequency and temperature ramp. It provides an insight into the load damping ability of polymer when subjected to a cycle of the dynamic load at a frequency and a temperature sweep. Apart from this, other properties like impact strength, Young's modulus hardness, %crystallinity, and others are also important to investigate the application of polymer as a metallic knee replacement in a prosthetic leg. The following section briefly discusses important literature in the area of dynamic mechanical properties' evaluation and also on important mechanical and thermal properties of hybrid polymer nanocomposites.

Badgayan et al. [5] reported on the application of HDPE reinforced with MWCNT and h-BNNP as fracture fixation plates and the acetabular cup. Melk et al. [6] studied the incorporation of CNTs, graphene (GO), and nanodiamonds (ND) on the mechanical and thermal properties of UHMWPE blended with vitamin E. The composites were reported to find application in for bearing components in joint arthroplasty. Ferreira et al. [7] investigated the dynamic mechanical properties of HDPE reinforced with three different types of functionalized CNTs. The storage and loss modulus was recorded to increase upon addition of dodecylamine-functionalized CNT as compared

to the other two. Rafiee et al. [8] reported an increase in storage modulus of neat polypropylene reinforced with organo-modified layered double hydroxide nanoparticles. Xiao et al. [9] evaluated the crystallization temperature of poly(vinylidene fluoride) (PVDF)-based nanocomposite and hybrid composite reinforced with CNT and GNP using differential scanning calorimetry (DSC). The highest crystallization temperature was shown by PVDF/CNT/5 wt% GNP which increased by 7.05 % in comparison with pure PVDF. Liu et al. [10] studied the storage modulus of HDPE reinforced with graphite nanofibers and graphite nanoplatelets using DMTA. At a temperature of -70 °C and room temperature, the storage modulus was observed to increase by 70 and 83 % in comparison with pure HDPE. Hwang et al. [11] investigated the thermal conductivity of poly(ether–ether–ketone) (PEEK) hybrid containing ethyl-aminated and phenyl-aminated graphene oxide (GO)/CNT (E-GC or P-GC) hybrid composite. The thermal conductivity was observed to increase at 1 wt% GO loading in comparison with neat PEEK. Jin et al. [12] reported on dynamic mechanical properties of epoxy-DGEBA reinforced with nano: Al_2O_3 and SiC. The storage modulus in the glassy and rubbery regions of both composites; DGEBA/Al_2O_3 and DGEBA/SiC increased with increasing filler content. Fouad et al. [13] investigated the application of high-density polyethylene and graphite nanoparticles for total hip joint replacements.

Based on the surveyed literature, it is found that none of the works reported on the context of HDPE reinforced with a multidimensional filler system. In this current work, HDPE is reinforced with 1D-multiwalled carbon nanotubes (MWCNTs) and 2D-hexagonal-boron nitride nanoplatelet (h-BNNPs) to form novel polymer composites and hybrids. The objective of the current work is to evaluate dynamic mechanical, thermal, and mechanical properties of prepared samples and to find application as a substitute for a metallic knee in a prosthetic leg. An attempt is also made to modify the Halpin–Tsai equation and Hamilton and Crosser model for effective prediction of Young's modulus and thermal conductivity and comparison with experimental results. The rationale behind selection of HDPE as matrix lies in its inherent high Young's modulus and both chemical and biological inertness. It had been used in both bone tissue engineering and bone reconstruction [14, 15]. The CNTs exhibit superior mechanical properties [16], whereas h-BNNPs exhibit superior tribological and thermal performance [17]. Apart from this, it brings unique 1D/2D geometry of nanofiller and this choice of filler brings unique B-C-N triad formation. The authors are keen to investigate these effects on the different properties' evaluation of composite samples.

2 Materials and Methods

2.1 Materials

The details of HDPE, MWCNTs, and h-BNNPS are referred to Badgayan et al. [18]. The TEM images of nanofillers as shown in Fig. 1a and b confirms the tubular and hexagonal morphology of MWCNT and h-BNNP. A mixture of MWCNT and h-BNNP is shown in Fig. 1c. The representation of nanofiller in HDPE could be visualized from Fig. 1d–f. Both the MWCNT and h-BNNP were surface modified as described by Sreekanth et al. [19] and Xie et al. [20], respectively.
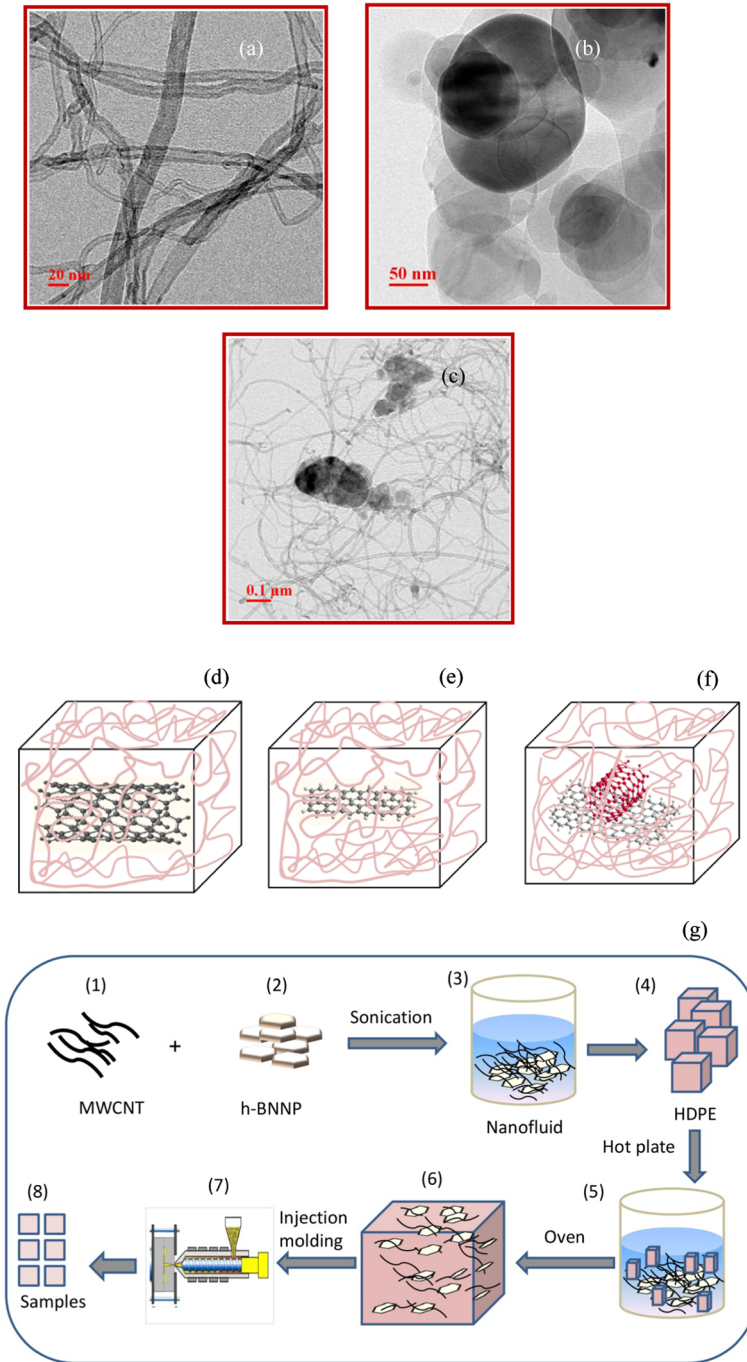
Fig. 1 TEM images of (a) MWCNT (b) h-BNNP; (c) h-BNNP/MWCNT hybrid nanofillers, and (d–f) hypothetical models showing interaction of filler system in matrix; (g) preparation route followed

Table 1 Composition of samples

Sample	wt%	Designation
MWCNT	0.1	C1
h-BNNP	0.1	C2
MWCNT/h-BNNP	0.25/0.1	H1
MWCNT/h-BNNP	0.25/0.15	H2

2.2 Preparation of Test Samples

A total of five samples were prepared including pure HDPE. The concentration of MWCNT and h-BNNP varied between 0.1 wt% and 0.25 wt% to prepare different composites and hybrids. The test samples were obtained using mechanical mixing and curing in a vacuum oven followed by an injection molding technique. The oven was hermetically sealed and samples were cured at a temperature of 100 °C for 24 h to remove any moisture traces from the samples. A total of two nanocomposites with equal loading of MWCNTs and h-BNNPs were prepared: 0.1 MWCNT and 0.1 h-BNNP; and two hybrid composites were prepared to assess the effects of individual fillers: 0.25 MWCNT/0.1 h-BNNP and 0.25 MWCNT/0.15 h-BNNP. The notation of the composites and hybrids is designated in Table 1. The detailed preparation procedure can be understood from Fig. 1g and any further details are attributed to Badgayan et al. [5].

2.3 Characterization

2.3.1 Dynamic Mechanical Thermal Analysis

DMTA analysis was performed on TA (DMA Q 800) instrument according to ASTM D4065-01 standard. The tests were performed in three-point bending mode which is regarded as a pure mode of deformation with the elimination of clamping effects using low friction roller bearing supports that improve accuracy. The tests were performed on a sample of final dimension $60 \times 12.5 \times 3$ mm^3 at a constant frequency of 1 Hz and a temperature ramp between 30 °C and 110 °C with a heating rate of 1 °C·min^{-1}.

2.3.2 Mechanical Properties

Micro-tensile specimens were obtained from the injection molding machine and test standard ASTM D1708 was followed to evaluate tensile properties. The tests were performed on an INSTRON 8801 tensile tester of dynamic load capacity ± 100 kN and load cell accuracy of 0.005 % at a crosshead speed of 1 mm·min^{-1} at ambient temperature. The repeatability of the result is ensured by testing five samples per material type. A Vickers diamond pyramid indenter HV-1000Z was deployed for microhardness studies. A total of five indentations were made on each test sample to ensure repeatability. The impact testing was carried out on Charpy impact testing mode with a maximum impact energy of 10 J. A JEOLJEM 2100 Transmission Electron

Microscope with an operating voltage of 200 kV was used to study the morphology of chemically treated CNT and h-BNNP.

2.3.3 Thermal Properties

Differential calorimetric studies and Thermogravimetric Analysis studies were carried out on a NETZSCH simultaneous thermal analyzer-model STA449F3 with power resolution of < 0.1 µW. The DSC analysis was carried out at a temperature swept between room temperature and 200 °C on a nitrogen gas atmosphere. The samples were in the form of pellet weighing 4–5 mg. The samples for TGA analysis were in the form of pellets weighing 4–5 mg and tested during a temperature ramp from 30 °C to 800 °C on nitrogen gas atmosphere. The nitrogen gas flow rate is maintained at 20 mL·min^{-1}. Thermal conductivity was determined using the Hot Disk Thermal Analyser-TPS 2500S with a specimen size of 10 mm in thickness and 30 mm in diameter.

3 Results and Discussion

3.1 Dynamic Mechanical Properties

3.1.1 Storage Modulus

The storage and loss modulus of all the tested samples is evaluated in the temperature range between 30 °C and 110 °C and shown in Fig. 2a, b. At a temperature of 36 °C, the storage modulus of pure HDPE is noted as 875.93 MPa which increased by 18.51 %, 6.41 %, 15.42 %, and 22.05 % in comparison with C1, C2, H1, and H2, respectively. Similarly, on a comparison of C1 with C2 nanocomposite with equal loading, it was observed that the storage modulus of C1 exceed that of C2 by ~ 12 %, while no significant variation was noted with hybrid H1. The highest storage modulus is noted for H2 hybrid composite over the entire tested range at 36 °C. It increased by 22.05 % in comparison with pure HDPE and an increase of 6.21 % in comparison with C1. It should be noted that at a temperature of 36 °C the storage modulus of H2 and C1 is noted as ~ 1068 MPa and ~ 1038 MPa. The difference is marginal and highest storage modulus acclaimed by C1. The reasons can be addressed as twofold: firstly good interfacial adhesion of CNT in the HDPE matrix [21]; secondly, CNTs are rolled up sheets of graphene with layers separated from each other by strong Van der Waals' force [22]. It should be understood that DMTA is bulk mechanical property evaluation technique and CNTs being 1D nanofiller with the only diameter limited to the scale of nanometers. When the load is applied in a sinusoidal manner, a large number of CNTs compress or deform temporarily and the applied load is stored in the form of energy and it is released upon removal of the load, thereby acclaiming large storage modulus. On the contrary, the storage modulus of C2 is observed as lowest after pure HDPE. The same is reasoned to morphology of h-BNNPs, which are ceramic nanoplatelets and exhibit good stiffness (Young's modulus is about 20 GPa). It should be noted
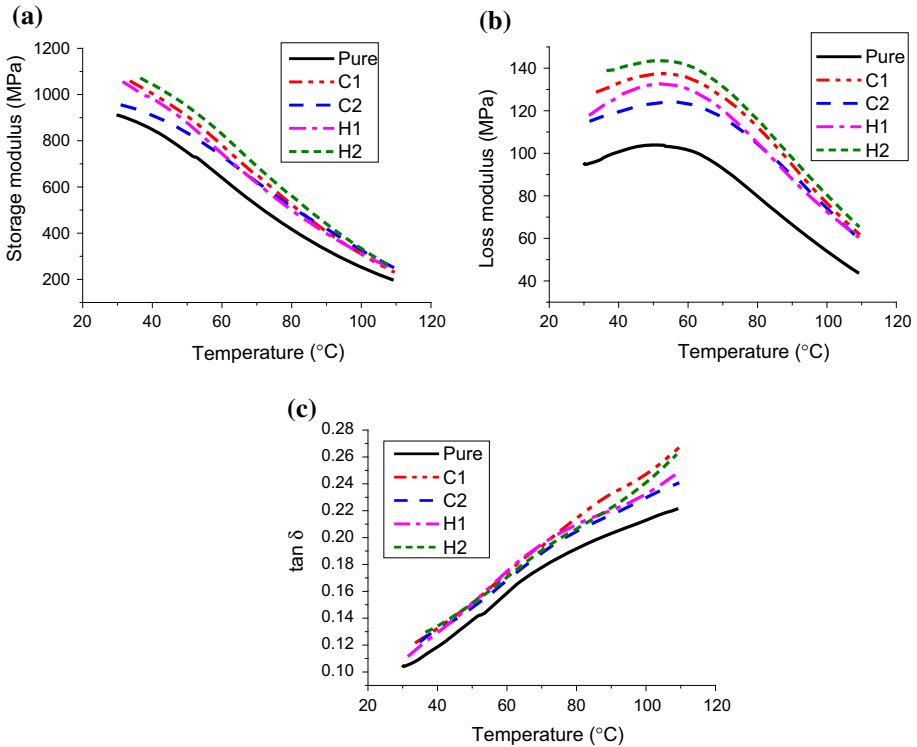
Fig. 2 (a) Storage modulus; (b) loss modulus; (c) tan δ vs. temperature of samples

that a stiff material is always difficult to deform elastically concerning directional orientation, thereby exhibiting small storage modulus.

3.1.2 Loss Modulus

Similarly, at a temperature of 36 °C the loss modulus of pure HDPE is noted as 95.09 MPa which increased by 35.86 %, 23.15 %, 29.60 %, and 45.16 % in comparison with C1, C2, H1, and H2, respectively. It is evident from Fig. 2b that the loss modulus of CNT-based composites and hybrids exhibited superior loss modulus in comparison with pure and C2 composite.

At a temperature of 36 °C, the loss modulus of C1 is enhanced by 35.78 %, 10.25 %, and 5.71 % in comparison with pure, C2, and H1. It also decreased by 6.41 % in comparison with H2. The possible reasons for a large loss modulus of C1 composite can be addressed from a twofold reason: firstly, the addition of CNT in HDPE leads a mesophase formation which dissipates energy from external stresses by frictions between particle–particle and particle–polymer interaction [7, 23]. Secondly, when the DMTA probe is removed from the CNT-based sample's surface owing to the rolled up cylindrical configuration of CNT, it starts to vibrate thereby dissipating the stored energy and acclaims large loss modulus. A small loss modulus of C2 composite

can be inferred from the reason; h-BNNP being ceramic nanoplatelets is difficult to deform elastically thereby it experiences low loss modulus and its inherent hardness enables fewer chances of dissipation of applied stored energy. It is also observed that at a temperature of 36 °C the storage and loss modulus is observed in the order: H2 > C1 > H1. The same is reasoned to an increase in CNT weight fraction; H1 and H2 have a small effect on both storage and loss modulus. At a temperature of 36 °C, the storage modulus and loss modulus of H1 increased by ~ 3.0 and ~ 4.0 % in comparison with C1. The storage and loss modulus, upon an increase in h-BNNP weight fraction from 0.1 to 0.15 in hybrid composite H2, results in an increase of ~ 3.0 and ~ 7.0 % in comparison with C1 composite. It can be inferred that an increase in CNT and h-BNNP weight fraction in the hybrid composites has small effects towards improvisation of storage and loss modulus. The reasons can be inferred from the fact that the number of CNT dispersed per unit volume in C1 composite is less than that when compared with H1 hybrid composites and similarly the number of h-BNNP dispersed per unit volume in H1 hybrid is less than that of H2. When the number of nanofillers is increased per unit volume, it offers sufficient resistance towards the applied deformation load, with an increase in resistance towards deformation the cushioning effect of CNT decreases and as CNTs are dispersed on h-BNNP it offers a rigid structure, thereby decreasing the storage and loss modulus abilities of both the hybrid composites.

The storage and loss modulus of all the test samples is evaluated during a temperature sweep between 30 °C and 110 °C. The storage modulus of C1 composite varied between 1055.52 MPa and 233.48 MPa which increased by 15 and 17 % in comparison with pure HDPE over the same tested range. Similarly, during a temperature sweep between 30 °C and 110 °C the loss modulus of C1 composite varied between 128 MPa and 62 MPa, which has increased by 40.65 and 44.18 % in comparison with pure during the same corresponding temperature range. The analysis of test results confirms optimum property acclaim by C1. However, with an increase in temperature between 30 °C and 110 °C both the storage and loss modulus of all the tested samples is observed to decrease. An intense dropout of storage and loss modulus is observed with increase in temperature indicating advent of the rubbery region [24]. The possible reasons can be attributed to the fact that at elevated temperature polymer loses its tight packing arrangement and molecular mobility increases which initiates flow behavior, and therefore a decrease in both storage and loss modulus is observed with increase in temperature.

3.1.3 Tan δ

Tan δ or damping ratio exonerates elastic and viscous behavior of a material. Tan δ peaks of the tested sample are elucidated in Fig. 2c. For pure, the Tan δ varied between 0.10 and 0.22 at a temperature sweep between 30 °C and 110 °C, which marks an increase of 120 %. On the contrary, for C1 composite, the Tan δ varied between 0.12 and 0.26 during the same temperature sweep marking an increase of 116 %. It is observed that at 30 °C, Tan δ exhibits minimum value for the entire tested samples. The values are closer to 0.1 confirming an elastic behavior of the tested samples. The reasons can be explained as follows: at low temperature, the molecular mobility of the polymer chains is limited and owing to the restricted mobility the stored energy

is unable to dissipate by internal friction. On the contrary at elevated temperature, polymer chain mobility increases which dissipates the stored energy through internal friction. The optimum tan δ exhibited by C1 composite, which exhibits best elastic behavior at low temperature at 30 °C and best damping property at 110 °C. The possible reason lies in the morphology of CNTs. It is a known concept that CNT length exceeds nanometer scale and it forms endless coiled tubular-like structure sometimes stacked one upon another. Apart from this, HDPE also possesses longer chain length and at elevated temperature, the integrated effects of HDPE and CNTs come into action. For HDPE reinforced with CNTs, at elevated temperature, the polymer chains become more mobile and start dissipating the energy thereby exhibiting large damping ratio.

3.2 Mechanical Properties

The load vs. displacement plot of samples is shown in Fig. 3a and it is evident from Fig. 3a that all the composite samples reach the yield point and draws further forming a neck and breaks finally. The steepest ascent is shown by H2 hybrid composite confirming the largest load required to cause deformation. The mechanical properties namely hardness and impact toughness are calculated and plotted in Fig. 3b, c. The hardness of pure HDPE is noted as 3.02 GPa, which increased by 17.88 and 42.38 % in comparison with C1 and C2. Similarly, an increase of 90.72 and 172.18 % is observed while comparing H1 and H2 with pure HDPE. The impact toughness of C1 and C2 composite is observed to increase by 26.09 and 77.56 % in comparison with pure HDPE. Similarly, an increase in 1.1- and 1.9-fold is observed when impact toughness of H1 and H2 is compared to pure HDPE, respectively. It should be observed that hardness and impact toughness of C2 composite is superior to C1. The possible reasons can be (a) h-BNNPs are ceramic nanoplatelets with one layer stacked upon another inheriting extraordinary hardness [25], (b) chemical treatment of h-BNNP modifies its surface and certain functional groups are attached to it, thereby enhancing good interfacial adhesion with HDPE. On the contrary, CNT also exhibits superior mechanical performance [16], but on comparing CNT with h-BNNPs, they are more flexible and pliable thereby exhibiting less hardness and impact toughness. However, H2 exhibited the highest hardness and impact toughness which can be inferred to a synergistic effect between nanofillers and HDPE. The h-BNNPs being 2D nanostructured platelet with thickness limited to nanoscale offers a strong rigid support on which CNTs are oriented randomly as they are 1D filler with a length exceeding nanometer. Apart from this, the strong interlayer Van der Waals' force of CNT become first to sustain the load of deformation and thereby transferring it to the rigid support of h-BNNP.

The Young's modulus is calculated from the stress vs. strain curve and plotted in Fig. 4a and it increased by 27.35 % for 0.1 CNT in comparison with pure HDPE. The possible reasons can be inferred from multiple rationales: (a) Young's modulus of CNT is theoretically 1.8TPa and chemical treatment of CNT ensures proper matrix nanofiller hybridization. (b) Young's modulus can be altered by substitution or insertion of atoms at lattice points [3]. The highest Young's modulus is observed as 1.52 GPa for H2
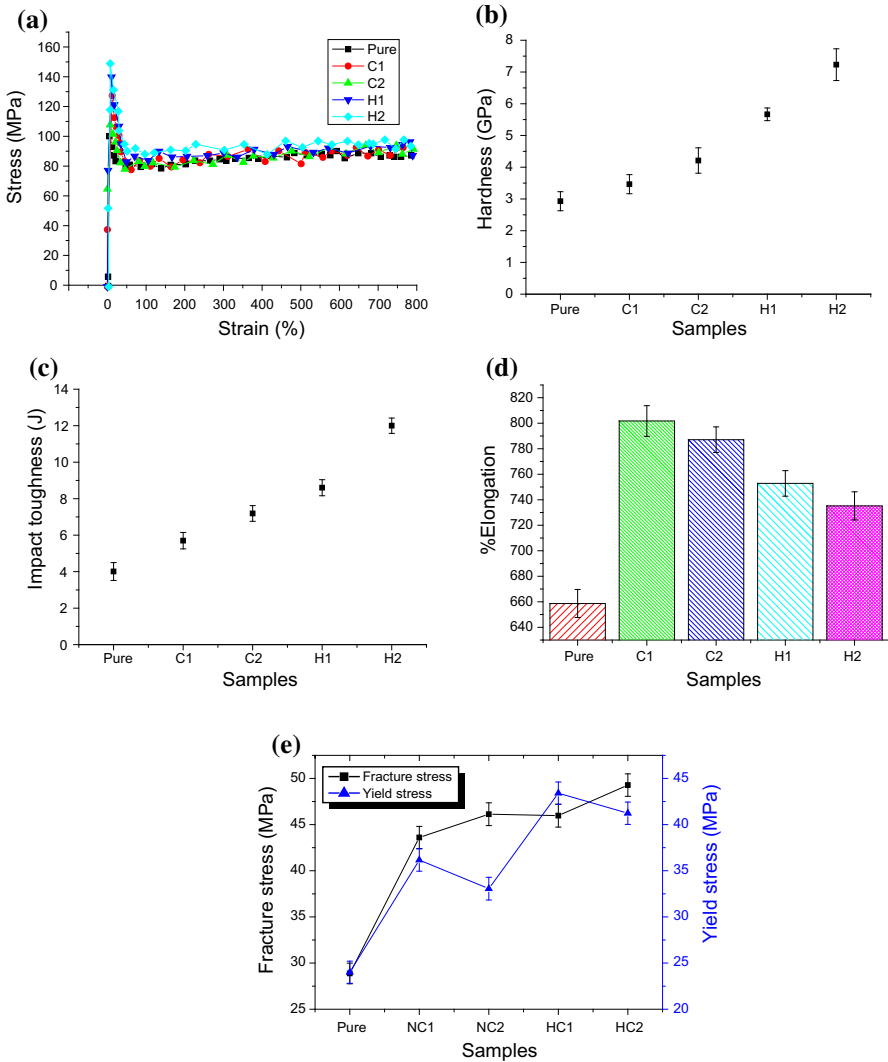
Fig. 3 (a) Stress vs. strain; (b) hardness; (c) impact toughness; (d) % elongation; (e) fracture stress vs. Yield stress vs. samples

hybrid which increased by 50 % in comparison with pure HDPE. It should be noted that H2 has exhibited optimum stiffness, hardness, and impact toughness.

The other mechanical properties like yield stress and fracture stress are shown in Fig. 3e. The yield stress of 0.1 CNT increased by 37.5 MPa and 10.18 % in comparison with pure HDPE and C2. The reasons can be addressed to its more elastic nature pertaining to large L/D ratio of CNT. In the case of H2, CNTs are dispersed randomly on an h-BNNP rigid support. Each h-BNNP layer is separated from each other by weak Van der Waals' force which causes easy gliding of one layer over another only once
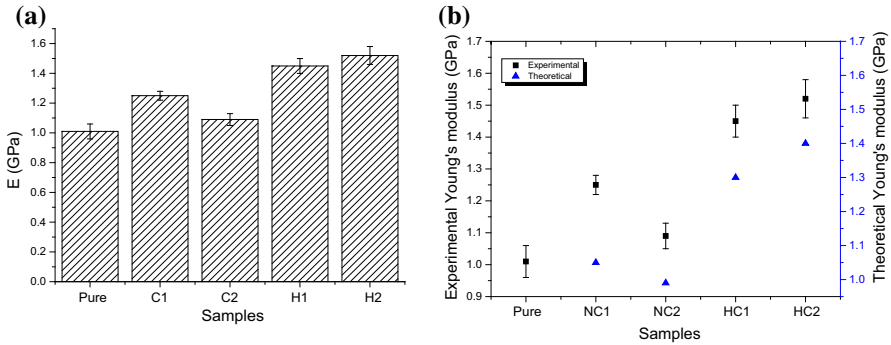
Fig. 4 (a) Young's modulus vs. samples; (b) experimental vs. theoretical predication Young's modulus vs. samples

the threshold load is reached. The integrated effects of h-BNNP and CNT pronounce more elasticity and stress at yield point. The %elongation at fracture for 0.1 CNT is noted as 801.86 which increased by 21.73 and 10.09 % in comparison with pure HDPE and H2. The results confirm elastic behavior of 0.1 CNT composite. However, the stress at fracture is noted as 49.30 MPa for H2 hybrid nanocomposite, which increased by 72.87 % in comparison with pure HDPE. It should be noted that apart from the reasons addressed for improvised mechanical property acclaim by different composites and hybrids the degree of crystallinity envisages an important role. Owing to the same differential calorimetry, studies are also carried out and discussed in the relevant section.

3.2.1 Theoretical Prediction of Young's Modulus

Numerous theoretical works are carried out for the prediction of Young's modulus of heterogeneous materials; however, most of them are limited to the prediction of the stiffness of fiber-reinforced composites using theoretical modeling or Finite Element Analysis. [26, 27]. Kanagaraj et al. [28] modified Halpin–Tsai equations for prediction of Young's modulus of particle-reinforced composite system containing single nanofiller.

In this section, the Halpin–Tsai equations are carefully modified to predict Young's modulus of the particulate-reinforced composite system with single and hybrid filler as well. The predicted values of Young's modulus are in close agreement with experimental test results for composites with both single and hybrid filler system as shown in Fig. 4b.

Young's modulus of CNT composite:

$$E_{C_1} = \frac{E_{CNT}}{E_m} = \frac{3}{8}\left[\frac{1 + 2\left(l/d\right)_{CNT}\eta_L\phi_{CNT}}{1 - \eta_L\,\phi_{CNT}}\right] + \frac{5}{8}\left[\frac{1 + 2\eta_T\,\phi_{CNT}}{1 - \eta_T\,\phi_{CNT}}\right], \quad (1)$$

where

$$\eta_T = \frac{\left(E_{CNT}/E_{HDPE}\right) - 1}{\left(E_{CNT}/E_{HDPE}\right) + 2} \eta_L = \frac{\left(E_{CNT}/E_{HDPE}\right) - 1}{\left(E_{CNT}/E_{HDPE}\right) + 2\left(l/d\right)_{CNT}}. \qquad (1.1)$$

Young's modulus of the h-BNNP composite:

$$E_{c2} = \frac{E_c}{E_m} = \frac{3}{8}\left[\frac{1 + {}^2/3\left(\frac{L_{BNNP}}{t_{BNNP}}\right)\eta_L\,\phi_{BNNP}}{1 - \eta_L\,\phi_{BNNP}}\right] + \frac{5}{8}\left[\frac{1 + 2\eta_T\phi_{BNNP}}{1 - \eta_T\,\phi_{BNNP}}\right], \qquad (2)$$

where

$$\eta_L = \frac{\left(E_{BNNP}/E_{HDPE}\right) - 1}{\left(\frac{E_{BNNP}}{E_{HDPE}}\right) + \frac{2}{3}\left(\frac{L_{BNNP}}{t_{BNNP}}\right)} \qquad (2.1)$$

$$\eta_T = \frac{\left(E_{BNNP}/E_{HDPE}\right) - 1}{\left(\frac{E_{BNNP}}{E_{HDPE}}\right) + 2} \qquad (2.2)$$

η_L : longitudinal Young's modulus, η_T : transverse Young's modulus, t: thickness. Young's modulus of hybrid composite:

$$E_{hyb} = E_h\,\phi_h + E_m\,\phi_m, \qquad (3)$$

where Young's modulus of a hybrid system:

$$E_h = E_{C_1}^{\phi_{CNT}} \times E_{C_2}^{\phi_{BNNP}}. \qquad (3.1)$$

The volume fraction of hybrid filler:

$$\phi_h = \frac{\rho_m \times W_{CNT}}{(\rho_m \times W_{CNT}) + (\rho_{CNT} \times W_m)} + \frac{\rho_m \times W_{BNNP}}{(\rho_m \times W_{BNNP}) + (\rho_{BNNP} \times W_m)} \qquad (3.2)$$

E_m, ϕ_m are Young's modulus and volume fraction of matrix.

3.3 Thermal Properties

3.3.1 Thermal Conductivity

The thermal conductivity of different tested samples is shown in Fig. 5a. The thermal conductivity of pure HDPE is noted as 0.42 W·Mk^{-1}, which increased by 35.71 %, 11.90 %, 90.47 %, and 95.23 % in comparison with C1, C2, H1, and H2, respectively. The increase in thermal conductivity of composites is with regard to the superior
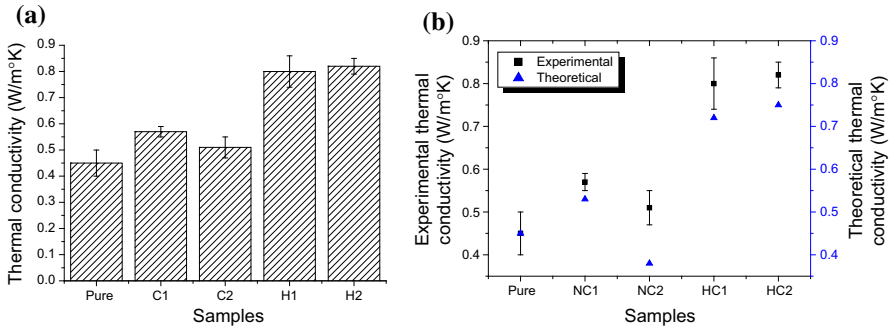
Fig. 5 (a) Thermal conductivity vs. samples; (b) experimental vs. theoretical prediction of thermal conductivity vs. samples

thermal conductivity of CNT and h-BNNP. The thermal conductivity of C2 decreased by 21.20 % in comparison with C1 which can be reasoned to low thermal conductivity, about 300 W·mK^{-1} possessed by h-BNNP on the contrary of 3000 W·mK^{-1} of CNT. On comparing composites with H2, a synergistic effect between nanofillers is observed which has raised thermal conductivity by 95.23 % in comparison with pure HDPE. It should be noted that aligned CNTs are excellent conductors of heat [29]. In the present case, 1D randomly oriented CNT is dispersed on 2D h-BNNP owing to the fact that intercalation of CNT into interlayer spacing of h-BNNP is unrealistic. Owing to the high aspect ratio of CNT, it effectively acts as an interconnector between each h-BNNP layers thereby forming a 3D heat conductive network and improvising the thermal conductivity. Apart from this, the crystallinity plays an important role in determining thermal conductivity. It is evident from the literature that an increase in crystallinity results in negligible thermal boundary resistance which improves thermal conductivity [30]. The DSC results confirm highest % crystallinity by 0.25 CNT/0.15 h-BNNP hybrid composite thereby exhibiting highest thermal conductivity.

Theoretical Analysis of Thermal Conductivity   A great deal of theoretical work is carried out towards mathematical modeling of thermal conductivity of composite materials [31, 32]. One of such primitive model is a Maxwell model which exonerates analytical formulations for predicting thermal conductivity heterogenic medium. However, it was limited to prediction of the small volume fraction of filler content. The Maxwell model was extended by Hamilton and Crosser model [33] which included different shape factors. In this current section, Hamilton and Crosser's model is successfully used to predict thermal conductivity of composites and a modified model predicts thermal conductivity of a composite system with hybrid filler. The comparison between the modified Hamilton and Crosser model and experimental values is shown in Fig. 5b. A close agreement between model and experimental value is observed with a mean absolute deviation of error limited to 0.01 signifying close fitting of data.

The thermal conductivity of CNT composite:

$$K_{C_1} = K_m \left[\frac{K_{CNT} + (n-1)K_m - (n-1)\phi_{CNT}(K_m - K_{CNT})}{K_{CNT} + (n-1)K_m + \phi_{CNT}(K_m - K_{CNT})} \right]. \tag{1}$$

Table 2 DSC analysis results for samples

Samples	T_m (°C)	T_c (°C)	χ_c (%)	h_f (J·g^{-1})	h_c (J·g^{-1})
Pure	132	116	50	92	149
C1	134	115	54	129	157
C2	137	115	58	133	169
H1	138	113	61	135	174
H2	142	112	72	178	199

The thermal conductivity of h-BNNP composite:

$$K_{C_2} = K_m \left[\frac{K_{BNNP} + (n-1)K_m - (n-1)\phi_{BNNP}(K_m - K_{BNNP})}{K_{BNNP} + (n-1)K_m + \phi_{BNNP}(K_m - K_{BNNP})} \right], \quad (2)$$

where Volume fraction [34] of CNT composite:

$$\phi_{CNT} = \frac{\rho_m W_{CNT}}{\rho_m W_{CNT} + \rho_{CNT} W_m}. \quad (2.1)$$

Volume fraction of h-BNNP composite:

$$\phi_{BNNP} = \frac{\rho_m W_{BNNP}}{\rho_m W_{BNNP} + \rho_{BNNP} W_m} \quad (2.2)$$

ρ_m = the density of matrix, ρ_f = density of filler, W_f = weight fraction of filler, W_m = the weight fraction of matrix, K_m = thermal conductivity of matrix, K_f = thermal conductivity of filler, n = empirical shape factor = $\frac{3}{\phi}$, ϕ = sphericity.

The thermal conductivity of the hybrid composite:

$$K_h = K_{C_1}^{\phi_{CNT}} + K_{C_2}^{\phi_{BNNP}}. \quad (3)$$

3.3.2 DSC Analysis

The melting temperature T_m, crystallization temperature T_c, the degree of crystallization X_c, latent heat of fusion, and crystallization are obtained through DSC analysis and shown in Table 2. DSC heating and cooling thermograms are shown in Fig. 6a, b. The melting temperature of pure HDPE is noted as 131.87 °C which is observed to increase on the addition of fillers. The highest melting point is exhibited by H2 hybrid composite which increased to 141.75 °C. The increasing trend of a melting point on the addition of fillers can be inferred to a large internal energy required to cause molecular mobility. The fillers in HDPE serves as a reinforcement which hinders the flow of heat thereby delaying the melting point. The inference is clearer with the large latent heat of melting value of composites in comparison with pure HDPE signifying increased heat required to cause melting. The enthalpy of melting of H2 increased by 92.39 % than pure HDPE. The latent heat of crystallization is obtained by integrating the area under the DSC cooling curve and shown in Fig. 6b. It is observed
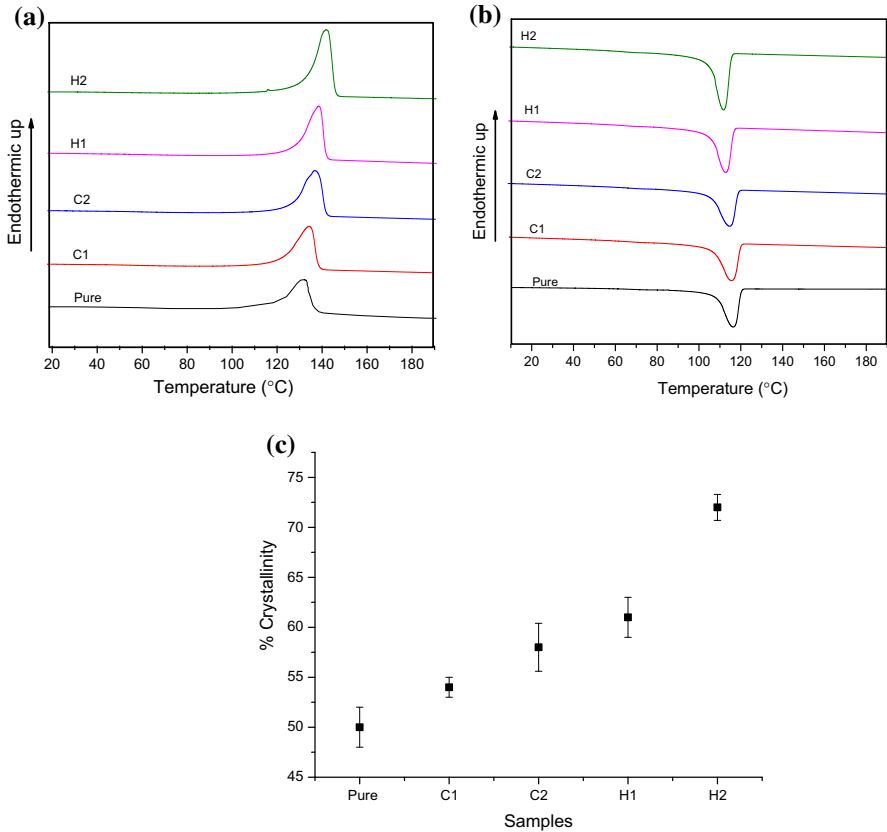
Fig. 6 (a) Heating; (b) cooling DSC curve of samples; (c) %crystallinity of samples

the enthalpy of crystallization of H2 hybrid nanocomposite increased by 34.45 % in comparison with pure HDPE signifying a larger amount of heat release. Similarly, for H2 hybrid, the T_c also shifted from 116 °C to 111 °C in comparison with pure HDPE confirming rapid nucleation and growth of several crystallites at the molecular level. The increase in crystallinity of samples can be observed in Fig. 6c, and it is observed that the crystallinity of pure HDPE is recorded as 50 %, which further increased to 54 %, 58 %, 61 %, and 72 % for C1, C2, H1, and H2, respectively. The increase in crystallinity of composites is due to fillers which acted as a site for nucleation of crystal growth [35].

3.3.3 Thermogravimetric Analysis

The TGA analysis of samples is shown in Fig. 7a, which shows the onset temperature of the tested samples. It is observed from Fig. 7a that the thermal stability of HDPE is increased significantly on the addition of fillers. The onset temperature of pure, C1, C2, H1, and H2 is noted as 144 °C, 165 °C, 177 °C, 286 °C, 322 °C as shown in Fig. 7c. The possible reason for an increase in onset temperature for composite samples lies
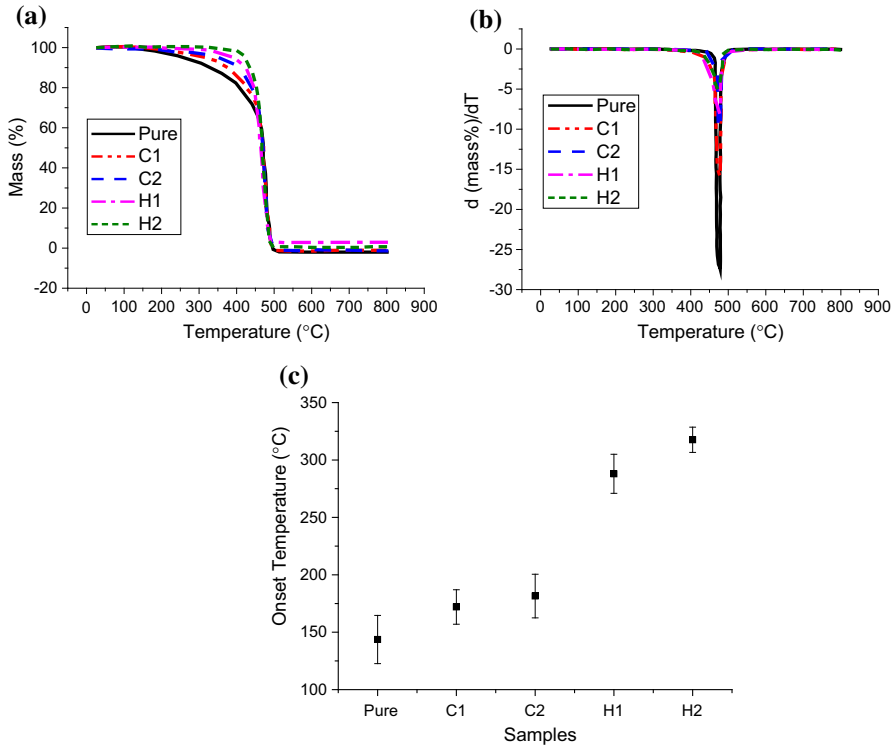
Fig. 7 (a) Mass% loss vs. temp.; (b) d (mass loss%)/dt vs. temp. of samples; (c) onset temp. of various samples

on the thermal conductivity of samples. An increase in thermal conductivity signifies more heat transfer which hinders the increase in sample's heat entrapment. The thermal conductivity of all the composite samples is noted higher than pure HDPE as already discussed in the relevant section. The oxidation temperature of the samples is found by differentiating the percentage of weight loss curve with temperature which is shown in differential thermogravimetric (DTG) as shown in Fig. 7b. The oxidation temperature H2 increased by 1.5 % in comparison with pure HDPE, whereas the weight loss % is noted as 5 % which is 27 % for pure HDPE. The possible reasons can be that the presence of high thermal conductivity fillers has dissipated heat properly which has nullified heat entrapment and acted as a barrier to degradation thereby preventing higher mass loss.

3.3.4 A Note on the Application

It is apparent that the properties of composite have improved with best being H2. However, based on the analogy, it can be noted that the increased/improved properties are on tandem with material properties required for prosthetic knee. The human knee or a prosthetic knee is a complex joint and it is subjected to loads in three dimensions

Table 3 Composites shown best performance

Property evaluated	Nanocomposite shown best performance	Hybrid nanocomposite shown best performance
Dynamic mechanical		
Storage modulus	C1	H2
Loss modulus	C1	H2
Loss factor (tan δ)	C1	H2
Thermal		
Thermal conductivity	C1	H2
Crystallinity	C2	H2
Thermal stability	C2	H2
Mechanical		
Hardness	C2	H2
Fracture stress	C2	H2
Yield stress	C1	H1
Young's modulus	C1	H2

and twisting moment in the same axes. A detailed analysis of the type of load and its intensity is referred to Bergmann et al. [36]. As discussed earlier in order to substitute a metallic knee with a polymer, the essential properties are high stiffness, hardness, damping ability, and thermal stability. In the present case, H2 hybrid nanocomposite has exhibited exceptional properties and the same is tabulated in Table 3.

4 Summary/Conclusion

The cardinal reasons for the evaluation of dynamic mechanical, thermal, and mechanical properties is to ascertain the applicability of the hybrid composite in a polycentric knee. The properties like storage and loss modulus, damping ratio, hardness, stiffness, impact toughness, thermal conductivity, crystallinity, and thermal stability were investigated. The following conclusion could be drawn from the results.

1. Superior mechanical properties like hardness, impact toughness, and stiffness were shown by 0.25 CNT/0.15 h-BNNP composite, thereby satisfying the prosthetic knee manufacturing essential criterion.
2. Thermal properties like thermal conductivity, %crystallinity, and thermal stability were noted as highest for 0.25 CNT/0.15 h-BNNP. This infers the ability of the prosthetic knee to withstand high temperature and ensure thermal stability.
3. 0.25 CNT/0.15 h-BNNP exhibited best damping abilities under dynamic loading. This ensures suitability of the prosthetic in situations like jogging, running, and sprinting.
4. Empirical models like Halpin–Tsai and Hamilton–Crosser were modified to fit stiffness and thermal conductivity. The test results confirmed that both the models could be used to predict the stated properties of hybrid composites as well.

It could be concluded that the fillers used as reinforcement had improvised different properties of composites and hybrids. The acclaim could be the result of synergy between HDPE-CNT-h-BNNP and B-C-N triad effects. The prosthetic knee proposed can possibly replace metallic knee and ensure ecqueonomies of manufacturing. However, the loading in the current work was 1D in contrast to 3D loading for a prosthetic knee. The critical behavior of the hybrid nanocomposite under physiological loading would be the subject of future.

References

1. N. Shahemi, S. Liza, A.A. Abbas, A.M. Merican, Long-term wear failure analysis of UHMWPE acetabular cup in total hip replacement. J. Mech. Behav. Biomed. Mater. **87**, 1–9 (2018). https://doi.org/10.1016/j.jmbbm.2018.07.017
2. C.T. Hsieh, C.Y. Liao, N.T. Dai, C.S. Tseng, B.L. Yen, S. Hsu, 3D printing of tubular scaffolds with elasticity and complex structure from multiple waterborne polyurethanes for tracheal tissue engineering. Appl. Mater. Today **12**, 330–341 (2018). https://doi.org/10.1016/j.apmt.2018.06.004
3. S.K. Sahu, N.D. Badgayan, S. Samanta, P.S.R. Sreekanth, Quasistatic and dynamic nanomechanical properties of HDPE reinforced with 0/1/2 dimensional carbon nano fillers based hybrid nanocomposite using nanoindentation. Mater. Chem. Phys. **203**, 173–184 (2018). https://doi.org/10.1016/j.matchemphys.2017.09.063
4. K.R. Kaufman, S. Frittoli, C.A. Frigo, Gait asymmetry of transfemoral amputees using mechanical and microprocessor-controlled prosthetic knees. Clin. Biomech. **27**, 460–465 (2012). https://doi.org/10.1016/j.clinbiomech.2011.11.011
5. N.D. Badgayan, S.K. Sahu, S. Samanta, P.S.R. Sreekanth, Assessment of nanoscopic dynamic mechanical properties and B-C-N triad effect on CNT/h-BNNP nanofillers reinforced HDPE hybrid composite using oscillatory nanoindentation: an insight into medical applications. J. Mech. Behav. Biomed. Mater. **80**, 180–188 (2018). https://doi.org/10.1016/j.jmbbm.2018.01.027
6. L. Melk, N. Emami, Mechanical and thermal performances of UHMWPE blended vitamin E reinforced carbon nanoparticle composites. Compos. Part B-Eng. **146**, 20–27 (2018). https://doi.org/10.1016/j.compositesb.2018.03.034
7. F.V. Ferreira, W. Franceschi, B.R.C. Menezes, F.S. Brito, K. Lozano, A.R. Coutinho, L.S. Cividanes, G.P. Thim, Dodecylamine functionalization of carbon nanotubes to improve dispersion, thermal and mechanical properties of polyethylene based nanocomposites. Appl. Surf. Sci. **410**, 267–277 (2017). https://doi.org/10.1016/j.apsusc.2017.03.098
8. F. Rafiee, M. Otadi, V. Goodarzi, H.A. Khonakdar, S.H. Jafari, E. Mardani, U. Reuter, Thermal and dynamic mechanical properties of PP/EVA nanocomposites containing organo-modified layered double hydroxides. Compos. Part B-Eng **103**, 122–130 (2016). https://doi.org/10.1016/j.compositesb.2016.08.013
9. Y. Xiao, W. Wang, X. Chen, T. Lin, Y. Zhang, J. Yang, Y. Wang, Z. Zhou, Hybrid network structure and thermal conductive properties in poly(vinylidene fluoride) composites based on carbon nanotubes and graphene nanoplatelets. Compos. PartA **90**, 614–625 (2016). https://doi.org/10.1016/j.compositesa.2016.08.029
10. T. Liu, B. Li, B. Lively, A. Eyler, W.H. Zhong, Enhanced wear resistance of high-density polyethylene composites reinforced by organosilane-graphitic nanoplatelets. Wear **309**, 43–51 (2014). https://doi.org/10.1016/j.wear.2013.10.013
11. Y. Hwang, M. Kim, J. Kim, Improvement of the mechanical properties and thermal conductivity of poly(ether-ether-ketone) with the addition of graphene oxide-carbon nanotube hybrid fillers. Compos. PartA **55**, 195–202 (2013). https://doi.org/10.1016/j.compositesa.2013.08.010

12. J. Jin, J.J. Lee, B.S. Bae, S.J. Park, S. Yoo, Jung, KH Silica nanoparticle-embedded sol-gel organic/inorganic hybrid nanocomposite for transparent OLED encapsulation. Org. Electron. **13**, 53–57 (2012). https://doi.org/10.1016/j.orgel.2011.09.008

13. H. Fouad, R. Elleithy, High density polyethylene/graphite nano-composites for total hip joint replacements: processing and in vitro characterization. J. Mech. Behav. Biomed. Mater. **4**, 1376–1383 (2011). https://doi.org/10.1016/j.jmbbm.2011.05.008

14. O.Y. Alothman, F.N. Almajhdi, H. Fouad, Effect of gamma radiation and accelerated aging on the mechanical and thermal behavior of HDPE/HA nano-composites for bone tissue regeneration. BioMed. Eng. OnLine **12**, 1–15 (2013). https://doi.org/10.1186/1475-925X-12-95

15. C. Kim, K. Jung, H. Kim, C. Kim, I. Kang, Collagen-grafted porous HDPE/PEAA scaffolds for bone reconstruction. Biomater. Res. **20**, 1–9 (2016). https://doi.org/10.1186/s40824-016-0071-5

16. M.M.J. Treacy, T.W. Ebbesen, J.M. Gibson, Exceptionally high Young's modulus observed for individual carbon nanotubes. Nature **381**, 678–680 (1996). https://doi.org/10.1038/381678a0

17. W. Cheewawuttipong, D. Fuoka, S. Tanoue, H. Uematsu, Y. Iemoto, Thermal and mechanical properties of polypropylene/boron nitride composites. Energy Proc. **34**, 808–817 (2013). https://doi.org/10.1016/j.egypro.2013.06.817

18. N.D. Badgayan, S. Samanta, S.K. Sahu, S.B.V. Siva, K.K. Sadasivuni, D. Sahu, P.S.R. Sreekanth, Tribological behaviour of 1D and 2D nanofiller based high density polyethylene hybrid nanocomposites: a run-in and steady state phase analysis. Wear **376–377**, 1379–1390 (2017). https://doi.org/10.1016/j.wear.2016.12.037

19. P.S.R. Sreekanth, S. Kanagaraj, Assessment of bulk and surface properties of medical grade UHMWPE based nanocomposites using nanoindentation and microtensile testing. J. Mech. Behav. Biomed **18**, 140–151 (2013). https://doi.org/10.1016/j.jmbbm.2012.11.011

20. B.H. Xie, X. Huang, G.J. Zhang, High thermal conductive polyvinyl alcohol composites with hexagonal boron nitride microplatelets as fillers. Compos. Sci. Technol. **85**, 98–103 (2013). https://doi.org/10.1016/j.compscitech.2013.06.010

21. P.S.R. Sreekanth, N.N. Kumar, S. Kanagaraj, Improving post irradiation stability of high density polyethylene by multi walled carbon nanotubes. Compos. Sci. Technol. **72**, 390–396 (2012). https://doi.org/10.1016/j.compscitech.2011.11.031

22. S.K. Sahu, N.D. Badgayan, S. Samanta, P.S.R. Sreekanth, Dynamic mechanical thermal analysis of high density polyethylene reinforced with nanodiamond, carbon nanotube and graphite nanoplatelet. Mater. Sci. Forum **917**, 27–31 (2018). https://doi.org/10.4028/www.scientific.net/MSF.917.27

23. W. Huang, Y. Wang, G. Luo, F. Wei, 99.9% purity multi-walled carbon nanotubes by vacuum high-temperature annealing. Carbon **41**, 2585–2590 (2003). https://doi.org/10.1016/S0008-6223(03)00330-0

24. N. Saba, M.T. Paridah, K.N. Abdan, A. Ibrahim, Dynamic mechanical properties of oil palm nanofiller/kenaf/epoxyhybridnanocomposites. Constr. Build. Mater. **124**, 133–138 (2016). https://doi.org/10.1016/j.conbuildmat.2016.07.059

25. R.S. Pease, An X-ray study of boron nitride. Acta Crystallogr **5**, 356–361 (1952). https://doi.org/10.1107/S0365110X52001064

26. C.L. Tucker, E. Liang, Stiffness predictions for unidirectional short fiber composites: review and evaluation. Compos. Sci. Technol. **59**(5), 655–671 (1999). https://doi.org/10.1016/S0266-3538(98)00120-1

27. M. Nasirshoaibi, N. Mohammadi, M. Nasirshoaibi, Mechanical properties of porous polymeric nanocomposites reinforced with mesoporous silica nanoparticles and hydroxyapatite: experimental studies and simulations. J Braz. Soc. Mech. Sci. Eng. **39**, 1721–1734 (2017). https://doi.org/10.1007/s40430-016-0602-y

28. S. Kanagaraj, F.R. Varanda, T.V. Zhiltsova, M.S.A. Oliveira, J.A.O. Simoes, Mechanical properties of high density polyethylene/carbon nanotube composites. Compos. Sci. Technol. **67**, 3071–3077 (2007). https://doi.org/10.1016/j.compscitech.2007.04.024

29. T. Evgin, H.D. Koca, N. Horny, A. Turgut, I.H. Tavman, M. Chirtoc, M. Omastova, I. Novak, Effect of aspect ratio on thermal conductivity of high density polyethylene/multi-walled carbon nanotubes nanocomposites. Compos. Part A **82**, 208–213 (2016). https://doi.org/10.1016/j.compositesa.2015.12.013

30. C.L. Choy, Thermal conductivity of polymers. Polymer **18**, 984–1004 (1977). https://doi.org/10.1016/0032-3861(77)90002-7

31. L. Rayleigh, On the influence of obstacles arranged in rectangular order upon the properties of a medium. Lond. Edinb. Dubl. Phil. Mag **34**, 481–502 (2009). https://doi.org/10.1080/14786449208620364
32. J.C. Maxwell, *A treatise on electricity and magnetism* (Oxford University Press, Oxford, 1904)
33. R.L. Hamilton, O.K. Crosser, Thermal conductivity of heterogeneous two component systems. Ind. Eng. Chem. Fundam. **1**, 187–191 (1962). https://doi.org/10.1021/i160003a005
34. M.E. Messiry, Theoretical analysis of natural fiber volume fraction of reinforced composites. Alex. Eng. J. **52**, 301–306 (2013). https://doi.org/10.1016/j.aej.2013.01.006
35. P.S.R. Sreekanth, S. Kanagaraj, Influence of MWCNTs and gamma irradiation on thermal characteristics of medical grade UHMWPE. Bull. Mater. Sci. **37**, 347–356 (2014). https://doi.org/10.1007/s12034-014-0640-y
36. G. Bergmann, A. Bender, F. Graichen, J. Dymke, A. Rohlmann, A. Trepczynski, M.O. Heller, I. Kutzner, Standardized loads acting in knee implants. PLoS ONE **9**, 1–12 (2014). https://doi.org/10.1371/journal.pone.0086035

Affiliations

Nitesh Dhar Badgayan[1,2] · Santosh Kumar Sahu[3] · Sutanu Samanta[2] · P. S. Rama Sreekanth[4]

[1]   Department of Mechanical Engineering, School of Technology, Assam Don Bosco University, Azara, Guwahati, Assam 781017, India

[2]   Department of Mechanical Engineering, North Eastern Regional Institute of Science and Technology, Nirjuli, Arunachal Pradesh 791109, India

[3]   Department of Mechanical Engineering, Amrita School of Engineering, Bengaluru, Amrita Vishwa Vidyapeetham, India

[4]   Department of Mechanical Engineering, Vellore Institute of Technology-AP University, Inavolu, Amaravati, Andhra Pradesh 522237, India